BILINGUAL PUBLISHING GROUP

Journal of Building Material Science

https://journals.bilpubgroup.com/index.php/jbms

REVIEW

Carbonation of Reinforced Concrete Sections Containing Various Supplementary Cementitious Materials: A Review

Mostafa Hassan

Construction and Building Engineering Department, Arab Academy for Science, Technology, and Maritime Transport (AASTMT), Alexandria 1029, Egypt

ABSTRACT

The rapid change in CO_2 concentration levels, due to climate change, will lead to a significant reduction in the durability and safety of the vital reinforced concrete (RC) structures. Utilizing supplementary cementitious materials, such as low calcium fly ash (LCFA) or slag, etc., with larger percentages in concrete mixes, would lead to an increase in the carbonation depth and risk of corrosion, especially for cracked concrete sections subjected to severe CO_2 concentration levels. This research aims to compare the carbonation depth values using two different mathematical models across various CO_2 concentrations and crack widths, for concrete mixes composed of different percentages and types of fly ash for both uncracked and cracked RC members, at a specific time of CO_2 exposure. Moreover, the main objective is to assess the probability of corrosion (PC) across various percentages and types of fly ash used in cracked RC decks subjected to a severe CO_2 level. The PC would be investigated through the Montecarlo simulation method. A Crack width of 0.1 mm in the RC decks would lead to a severe impact on the PC conducted using the Al-Ameeri model compared to the Kwon and Na model, when the percentages of LCFA vary from 5% to 30% in concrete mixes. It is recommended in this research to reduce the amount of high calcium fly ash in the mixes for RC decks to a percentage below 15% instead of LCFA to inhibit the carbonation-induced corrosion and enhance the durability and serviceability of RC structures.

Keywords: Cracked Concrete; Crack Width; Supplementary Cementitious Materials; High Calcium Fly Ash; Low Calcium Fly Ash

*CORRESPONDING AUTHOR:

Mostafa Hassan, Construction and Building Engineering Department, Arab Academy for Science, Technology, and Maritime Transport (AASTMT), Alexandria 1029, Egypt; Email: hassan92mostafa@yahoo.com or hassan92mostafa@aast.edu

ARTICLE INFO

Received: 17 September 2025 | Revised: 9 October 2025 | Accepted: 23 October 2025 | Published Online: 8 December 2025
DOI: https://doi.org/10.30564/jbms.v7i4.12144

CITATION

Hassan, M., 2025. Carbonation of Reinforced Concrete Sections Containing Various Supplementary Cementitious Materials: A Review. Journal of Building Material Science. 7(4): 142–161. DOI: https://doi.org/10.30564/jbms.v7i4.12144

1. Introduction

The durability and resilience of reinforced concrete (RC) structures, particularly bridge members, are fundamental to the integrity of transportation infrastructure. As critical components in supporting the mobility of people and goods, these structures are increasingly threatened by environmental degradation, primarily due to chloride or carbonation-induced corrosion. Climate change intensifies these threats, as rising temperatures and increased CO_2 concentrations accelerate degradation processes, posing long-term risks to the sustainability and safety of infrastructure. Moreover, climate change has significantly impacted the performance and service life of infrastructure worldwide. Climate-related stressors are already challenging; climate change exacerbates these conditions. Climate-induced conditions such as fluctuating temperatures, snow loads, heavy precipitation, ice accretion, and strong winds degrade the durability of structures, increasing the likelihood of failure[1]. The consequences of these changes extend beyond the design of new structures to the assessment and maintenance of existing ones[2]. The impact of climate change on infrastructure is primarily driven by different emission scenarios of greenhouse gases (GHG), aerosols, and land-use changes. Carbon dioxide (CO_2), a primary GHG, is considered the most significant contributor to global warming and the projected change in radiative forcing[3,4]. Under the most severe scenario, RCP8.5, CO_2 concentrations are projected to exceed 900 ppm, with a corresponding global temperature increase between 2.8 °C and 5.75 °C by the year 2100[5,6].

The corrosion of conventional carbon steel rebars embedded in concrete structures is considerably different from the corrosion of steel exposed to the atmosphere, as the reinforcing rebar is protected by the concrete cover, which acts as a barrier against the penetration of aggressive agents, especially for chloride ions, CO_2, water, and oxygen needed for the corrosion initiation and propagation stages. Corrosion in concrete structures can be described as a two-stage process according to Alhede et al.[7]: (i) corrosion initiation and (ii) corrosion propagation. Several studies conducted by Syll and Kanakubo[8] and Lin et al.[9] showed that the consequences of carbonation/chloride-induced corrosion in RC structures are as follows: loss of bond between the steel rebars and adjacent concrete, loss of ductility for steel rebars. Furthermore, the stresses generated due to corrosion products will lead to cracks and spalling of the concrete cover, which would reduce the service life of RC structures.

The carbonation of the concrete is the combination of physical and chemical processes[10,11]. The main factors affecting carbonation of concrete are the type of cement and its content, cement composition, the water-to-binder ratio, CO_2 diffusivity within the concrete pores, CO_2 concentration, the maximum temperature, and the relative humidity[12,13]. The carbonation depth (CD) increases with the increase in the relative humidity and reaches the peak when the relative humidity is in the range of 60–70%[14]. Elsalamawy et al.[14] found that the factor of relative humidity in the Chinese carbonation model is the most effective model, considering various relative humidity ranges, compared to other mathematical models that are restricted to RH% ranges from 60–100%. The effect of temperature on the diffusion coefficient is modeled using the Arrhenius law[11,13,15,16]. The higher temperature will cause an increase in the diffusion coefficient, leading to increased CDs[11].

The primary concern with concrete carbonation is the increased CO_2 levels due to climate change, which could significantly compromise the durability of concrete structures by accelerating CD. This would pose serious challenges to the long-term functionality and safety of critical infrastructure. With the increase in CO_2 levels due to global warming, RC structures in urban environments face increased risk. Consequently, concrete quality, cement content, and cover thickness are critical in resisting carbonation.

To mitigate the consequences of carbonation-induced corrosion in RC structures, specific requirements are recommended in the future:

- Reducing the water-to-cement ratio in the concrete mix must be considered to produce low-permeability concrete and a more resistant concrete microstructure against carbonation/chloride-induced corrosion.
- Providing adequate concrete cover for the reinforcement that satisfies specific minimum requirements according to the standard code.
- Utilizing galvanized steel or stainless steel rebars instead of carbon steel rebars to inhibit the corrosion of steel rebars, especially for vital RC structures.
- Using barrier coatings (i.e., powder, plastic, and paint) to adhere to metal surfaces must be recommended for steel rebars exposed to corrosive environments.

- Utilizing geopolymer concrete made of sustainable materials instead of normal concrete for RC members exposed to extreme environmental conditions to increase the service life and durability of the RC structures, according to Amleh et al.[15].
- Using a calcium nitrite-based corrosion inhibitor is associated with the optimum percentage of fly ash (FA).

The probability of carbonation-induced corrosion for the uncracked RC member subjected to the CO_2 level after 50 years of exposure was found to be negligible according to Schultheiß et al.[17]. The influence of crack width increases the carbonation depth significantly according to Forsdyke and Lees[18]. The cracks with openings below 0.05 mm increase the carbonation depth significantly, based on Varzina et al.[19]. The gap for this research is to assess the impact of various percentages and types of FA utilized as SCM in concrete mixes for cracked RC decks having various crack widths on the probability of carbonation-induced corrosion initiation (PCICI) at a specific time of CO_2 exposure using two different mathematical carbonation models. Moreover, the CD values across different CO_2 concentrations and crack widths will be calculated using two different mathematical models to show the variation between these two models.

This review study on carbonation-induced corrosion will aim to the following:

- Comprehensive review for various mathematical models utilized in conducting CD values for concrete mixes, including various types and amounts of cement, water-to-cement ratios, and types and percentages of FA as supplementary cementitious materials (SCM), for cracked and uncracked RC sections at different times of CO_2 exposures.
- A review of the impact of various SCMs utilized as a partial replacement for the amount of cement used in concrete mixes on the CD of concrete.
- The latest review of the various methods for the prediction of the PCICI for uncracked and cracked concrete sections.
- A comparison study between two CD mathematical models for cracked concrete composed of various FA types and percentages will be illustrated.
- The impact of various crack widths and CO_2 concentrations on the concrete CD for concrete mixes composed of different types and percentages of FA at different times of CO_2 exposures, for uncracked and cracked concrete sections.
- Investigation of the PCICI across various types and percentages of FA using two mathematical models for cracked concrete sections with different crack widths will be further elaborated in detail.

2. Corrosions in Reinforced Concrete Structures: Carbonation of Concrete

Carbonation is the chemical reaction between carbonic acid (H_2CO_3) and calcium ions (Ca^{2+}) from the dissolution of hydrated cement products[20,21]. The reactions leading to the formation of calcium carbonate ($CaCO_3$) are shown in the progression of the chemical response of Equations (1) to (4)[22,23]. As atmospheric CO_2 concentration increases, the pH value of the concrete is reduced to approximately 8.0[22,24]. Then, the protective layer around the steel rebar is destroyed, and the steel is exposed to corrosion[25]. The deterioration of concrete structures is accelerated by climate change, primarily due to changes in CO_2 concentration, maximum temperature, and relative humidity. Moreover, the use of low-calcium fly ash ranging from 20–30% as SCM in the concrete mix, and the presence of cracks would accelerate the carbonation depth of the concrete[26]. The influence of carbonation on the environment has been studied by several researchers[13,26–28]. The increase in maximum temperature levels will cause an acceleration in the diffusion coefficient within the concrete microstructure, leading to increased CD[11].

$$CO_2 + H_2O \rightarrow H_2CO_3 \quad (1)$$

$$Ca(OH)_2 + H_2CO_3 \rightarrow Ca_2CO_3 + H_2O \quad (2)$$

$$3CaO{:}\,2\,SiO_2.3H_2O + 3H_2CO_3 \rightarrow 3\,CaCO_3 + 2\,SiO_2 + 3H_2O \quad (3)$$

$$4CaO{:}Al_2O_3.13H_2O + 3H_2CO_3 \rightarrow 4CaCO_3 + 2\,Al(OH)_3 + 10\,H_2O \quad (4)$$

where $Ca(OH)_2$ = Calcium Hydroxide; $3CaO{:}\,2\,SiO_2.3H_2O$ = Calcium-Silicate-Hydrate, SiO_2 = Silicon dioxide; $Al(OH)_3$ = Aluminum hydroxide.

Incorporating SCM, such as FA, silica fume (SF), and slag (SG), into concrete mixes can enhance durability[29]. SF can reduce CD[30]. The diffusion rate in concrete using

ordinary Portland cement (OPC) could be reduced to 2–5 times using mineral admixtures, especially SG cement[31]. These materials fill concrete pores and create a denser structure. Elevated temperatures accelerate corrosion processes, reinforcing the urgency of designing with resilience in mind. Hassan et al.[26] deduced that the influence of CO_2 concentrations ranging from 200 to 600 ppm applied on cracked concrete cover of 50 mm or beyond, having a crack width of 0.2 mm on the PCICI values, has a negligible impact when utilizing 30% of either high or low calcium FA as SCM at the age of 100 years of CO_2 exposure. However, the effect of using 30% Low Calcium FA (LCFA) as SCM in the concrete mix for an RC deck with a concrete cover of 50 mm is significant on the PCICI values compared to High Calcium FA (HCFA) with the same percentage at T = 100 years, when the CO_2 concentration varied from 600 to 1200 ppm applied on the top part of cracked RC deck.

3. Method of Estimation of the Carbonation Degree

The carbonation degree is investigated based on the CD, which depends on the pH value of the hardened concrete. The carbonation degree is not easy to measure. Moreover, a few qualitative techniques utilized to determine CD are based on pH value and phase analysis. The most popular indicator used for observing the CD is phenolphthalein[32,33]. The pH value of carbonated concrete is usually around 8.0, depending on the carbonation degree. The change in pH value reflects the carbonation degree according to the type of indicators used[34–40].

Many studies have shown that phenolphthalein is the most popular indicator because it can change colour in a pH range between 8.3 and 10 and is more accessible than other indicators[41–43]. The non-carbonated concrete zone will appear pink and clear when carbonated. However, the main disadvantage of using phenolphthalein as an indicator is the difficulty in detecting the partially carbonated zone where the pH is more than 10. The proposed two new indicators, which show a change in colour at the higher pH value, are alizarine yellow R and indigo carmine, which transfer their colour from blue to yellow at a pH value of 10.0 to 11.4. Therefore, it was deduced that these new indicators could provide higher accuracy and dependability in the alkalinity measurement of the partially carbonated zone, as they could detect carbonated zones.

4. A Comprehensive Review of the CD Projections Using Various Mathematical Models

This section shows a review of a summary of existing studies related to the calculation of the front depth of carbonation and time of corrosion initiation using various mathematical models for cracked and uncracked concrete sections, as shown in **Table 1**. The mathematical models for the conduction of CD are based on different parameters. Moreover, the parameters that affect CDs are as follows: types of cement, cement composition, cement hydration, water-to-cement ratio, amount of water, effective diffusivity of CO_2, curing process, maximum temperature, relative humidity, crack width, compressive strength of concrete, types and percentages of SCM, and time of CO_2 exposure.

The mean values for the diffusion coefficients and age factors utilized in Yoon et al.[27] and Stewart et al.[44] CD models are based on experimental and field data. Moreover, the mean values for both diffusion coefficients and age factors are based on temperature (T = 20 °C) and relative humidity (RH = 65%) according to Sanjuán and del Olmo[45] and de Larrard[46]. The diffusion coefficients for CO_2 used in Yoon et al.[27] and Stewart et al.[44] vary in their values based on the types of climate regions, based on the Australian code AS3600[47].

Table 1. Different mathematical carbonation depth formulas for various types of RC sections.

CD Mathematical Models	References	Types of RC Section
$X_c(t) = k\sqrt{t}$ k: carbonation rate (mm/$\sqrt{y}$) in time (t).	Alhede et al.[7] & Lagerblad[48]	Uncracked Concrete
$X_c(t) = \sqrt{\frac{2D_{CO_2}\left(\frac{C_{CO_2}}{100}\right)t}{a}}$ a: amount of CO_2 uptake to complete carbonation by assuming 0.75 of hydrated cement could carbonate.	CEB-FIP[49] & Dyer[50]	

Table 1. *Cont.*

CD Mathematical Models	References	Types of RC Section
$X_c(t) = 1650 \times \left(\frac{w}{c} - 0.38\right) \times \left(1 - \frac{RH}{100}\right) \times (Y_{CO2}\ t)^{\frac{1}{2}}$	Morinaga [51]& Idem [52]	Uncracked Concrete W/C < 0.6
$X_c(t) = 150 \times \left(\frac{r_c\ K\ D}{f_c}\right) \times \sqrt{t}$	Bob and Afana [53]	Uncracked Concrete Parameters are illustrated in **Tables 2** and **3**.
$X_c(t) = \sqrt{\frac{2 \times D_{C02}}{a} \times t \times C}$ D_{CO2}: diffusion coefficient (cm^2/sec), a: CO_2 to complete carbonation, C: atmospheric CO_2 concentration (g/cm^3).	CEB-FIP [54]	Uncracked Concrete
$X_c(t) = \sqrt{2 \times K_e \times K_C \times C_s \times R_{NAC,O}^{-1}} \times W(t) \times \sqrt{t}$ $K_e = \left\{ \frac{\left[1-\left(\frac{RH_{real}}{100}\right)^5\right]}{\left[1-\left(\frac{65}{100}\right)^5\right]} \right\}^{2.5}$ $K_c = \left(\frac{t_c}{7}\right)^{b_c}$ $C_s = C_{s,\,atm} + C_{s,\,emi}$ $R_{NAC,O}^{-1} = ((K_t \times R_{ACC,O}^{-1}) + \varepsilon_t)$ $W(t) = \left(\frac{t_{o*}}{t}\right)^{\frac{(psr+T_{ow})^{bw}}{2}}$	CEB-FIP [55]	
$X_c(t) = 3\ K_{CO_2} \times K_{k1} \times K_{kt} \times K_{ks} \times K_F \times T^{0.25} \times K_{RH} \times \left(\frac{58}{f_{cuk}} \times 0.76\right) \times \sqrt{t}$ $K_{CO_2} = \sqrt{\frac{C_o}{0.03}}$ $K_{RH} = RH^{1.5} \times (1 - RH)$	CECS [56]	
$X_c(t) = 839\ (1 - RH)^{1.1} \sqrt{\frac{\frac{w}{c} \times r_c - 0.34}{r_{HD} \times r_c \times C}}\ C_0 \times \sqrt{t}$ t: time of exposure (days)	Jiang et al. [57]	Uncracked Concrete
$x_c(t) = \sqrt{\frac{2\ D_{e,CO2} \times \left(\frac{CO_2^*}{100}\right) \times t}{0.218 \times (C + (k^* \times P))}} = A_1$ $D_{e,CO2} = 6.1 \times 10^{-6} \left(\frac{\frac{[w - 0.267C - 0.267\ kP]}{1000}}{\frac{C+kP}{\rho_c} + \frac{w}{\rho_w}} \right)^3 \times f(RH)$ f(RH) = $(1 - (RH/100))^{2.2}$ $f(T) = exp\left[\frac{U_c}{R} \times \left(\frac{1}{T_{ref}} - \frac{1}{T}\right)\right]$ (The crack effect isn't considered.) $f(T) = exp\left[\frac{U_c}{R} \times b \times \left(\frac{1}{T_{ref}} - \frac{1}{T}\right)\right]$ (Cracks effect is considered based on Al-Ameeri et al. [58])	Papadakis & Tsimas [59], and Kwon & Na [60]	
$X_c(t) = \left(2.816 \times \sqrt{W_c} + 1\right) \times A_1$	Kwon and Na [60]	Cracked Concrete (W_c ranges from 0.1 mm to 0.20 mm).
$X_c\ (t) = (11.4 \times \sqrt{W_c} + 1) \times A_1$	Al-Ameeri et al. [58]	Cracked Concrete (W_c ranges from 0.05 to 0.35 mm).
$X_c(t) = \sqrt{\frac{2\ D_{co2}(t)}{a}\ K_{urban}\ C_{co2}\ (t - 1999)} \times \left(\frac{t_o}{t-1999}\right)^{n_m}$ $D_{co2}(t) = D_1 \times (t - 1999)^{-n_d}$ $a = 0.75 \times C \times C_a o \times \alpha_h \times \frac{M_{co2}}{M_{cao}}$ $\alpha_H \approx 1 - e^{-3.38w/c}$, according to de Larrard [46] $F_T(t) = e^{\frac{E}{R}\left(\frac{1}{293} - \frac{1}{273+Tav(t)}\right)}$, according to Yoon et al. [27] $T_{av}(t) = \frac{\sum_{i=2000}^{t} T(t)}{t-1999}$ D_1: CO_2 diffusion coefficient after one year, based on Sanjuán and del Olmo [45] and de Larrard [46].	Yoon et al. [27]	Uncracked Concrete $t \geq 2000$
$X_c(t) = \sqrt{\frac{2\ f_T(t) \times D_{co2}(t)}{a}\ K_{urban} \int_{2000}^{t} C_{co2}\ (t)\ dt}\ \ \left(\frac{1}{t-1999}\right)^{n_m}$	Yoon et al. [27] and Stewart et al. [44]	Uncracked Concrete $t \geq 2000$
$X_c\ (t) = k_w \times t^{1/2}$ $k_w = (3.355 \times c) - (0.019 \times C) - (0.042 \times fc) + 10.83$	Silva et al. [61] & Mizzi et al. [62]	Uncracked Concrete Restricted RH > 70%
$X_c(t) = \begin{cases} k\ k_g k_s \sqrt{\frac{\frac{w}{c} - 0.25}{0.3 \times \left(1.15 + 3\left(\frac{w}{c}\right)\right)}}\ \sqrt{t} & \frac{w}{c} > 0.6 \\ k\ k_g k_s \times \frac{4.6 \times \left(\frac{w}{c}\right) - 1.76}{\sqrt{7.2}}\ \sqrt{t} & \frac{w}{c} \leq 0.6 \end{cases}$	Koichi [63]	Uncracked Concrete -Various water-to-cement ratios. -Various cement content types.

Nomenclature for variables in **Table 1**:

A_1: carbonation velocity,
b: adjustment factor for cracks, equal to 0.322.
b_c: regression exponent, which is equal to −0.567 according to the fib model.
b_w: regression exponent, which is equal to 0.446,
C_{CO2}: atmospheric CO_2 concentration %,
C_o: is the Concentration of CO_2 (%).

C: cement content (kg/m^3),

c:CO_2 content (%),
$C_{s,\,atm}$: CO_2 concentration of the atmosphere, which in the fib model is equal to 0.00082 kg $_{CO2}$/ m^3.
$C_{s,emi}$: additional CO_2 concentration due to emission source (kg$_{CO2}$/m^3),

C_s: CO_2 concentration (kg /m^3),

CaO: calcium oxide content in cement (0.65),

C_e: cement content (kg/m^3),

CO_2*: CO_2 content in the ambient air at the concrete surface (%).
C_{CO2}(t): time-dependent mass concentration of CO_2 (1ppm = 0.0019 × 10^{-3} kg/m^3), and 1 mole of CO_2=44.01 grams,

D_{CO2}: CO_2 diffusion coefficient,

D_{CO2} (t): CO_2 diffusion coefficient in concrete over time (t),
$D_{e,\,CO2}$: effective diffusion coefficient for CO_2 (m^2/s),

E: activation energy of the diffusion process (40 kJ/mol),

f_c: concrete compressive strength (MPa),

f_{cuk}: cube compressive strength.
f(RH): influential factor of diffusivity of CO_2 in concrete due to relative humidity,
K_{urban}: the factor that accounts for increased CO_2 levels in urban environments.
k*: efficiency factor, which represents the resistivity against carbonation.
k_w is the carbonation coefficient (mm/year$^{0.5}$).

K_{kl}: Location factor, 1.4 for the corner and 1.0 for other places.

K_{Kt}: Factor of curing and casting factor, and is equal to 1.2.
K_{KS}: Stress factor, 1.1 for tension, 1.0 for compression.
K_F: FA replacement factor.
K_e: environmental function, which considers the influence of the relative humidity of the atmosphere.
K_c: execution transfer parameter, which considers the influence of the adopted curing measures.

k: the coefficient of influence of cement variety.

k_g: the coefficient of influence of aggregate variety,
k_s: the coefficient of influence of concrete additives.

K_t: test-method factor average value is equal to 1.25.

M_{CaO}: molar mass of the calcium oxide (56 g/mol),
M_{CO2}: molar mass of CO_2 (44 g/mol),
n_d: age factor for the CO_2 diffusion coefficient,
n_m: age factor for microclimatic conditions equals 0 for sheltered outdoors and 0.12 for unsheltered outdoors.
P: amount of SCM (kg/m^3),
p_{sr}: Probability of driving rain on the surface of the considered structure element.

R: gas constant (8.314 J/mole. K),

RH%: relative humidity percentage, and it is expressed as a fraction with a value greater than 50%. RH_{real}: relative air humidity,
$R^{-1}_{NAC,O}$: the inverse effective carbonation resistance of concrete obtained under natural conditions (NAC)(mm^2/year)/(kg$_{CO2}$/ m^3),
$R^{-1}_{NAC,O}$: the inverse carbonation resistance of concrete in an accelerated test under laboratory conditions.

r_{HD}: coefficient of the degree of hydration, and it is equal to 0.85 for 28 days of curing, 1.0 for 90 days of curing.
T_{ref}: reference temperature (298 K),
T: temperature of interest (K),
t_o: one year,
t: time of exposure (years),
t_o^*: reference time (years), its value is equal to 0.0767 years, which means the age at which the acceleration test is performed.
T_{ow}: time of wetness, which is the annual frequency of days with significant rainfall.
t_c: period of curing (days),
U_C: diffusion activation energy, the activation energy for CO_2 diffusing in concrete, has been experimentally determined as 39,000 J/mole.

W/C: water-to-cement ratio used.

W_c: crack width (mm),

W(t): weather function, which considers the influence of atmospheric precipitation on concrete carbonation.
X_c(t): CD over time (mm),
Y_{CO2}: ambient CO_2 content by volume (mol/m^3),
α_H: Degree of hydration,
ρ_c: density of cement, and it is equal to 3100 kg/m^3 according to Papadakis and Tsimas [59].

ρ_w: density of water (1000 kg/m^3),

ε_t: Error term with an average value equal to 315.5 ((mm^2/year)/(Kg/m^3)).

The relative humidity levels, CO_2 concentrations, and cement type factors utilized in Bob and Afana's [53] carbonation depth mathematical model are illustrated as shown in **Tables 2** and **3**.

Relative humidity factors at different levels are calculated using a mathematical equation based on the experimental tests conducted by Papadikas and Tsimas [58] (see **Figure 1**).

Table 2. Factors for various RH% and CO_2 emissions used in the CD model.

Relative Humidity (%)	**K**
RH% < 60%	1.00
70% < RH% < 75%	0.70
80% < RH% < 85	0.50
RH% > 90%	0.30
CO_2 Concentration	**D**
CO_2 < 0.03%	1.00
0.03% < CO_2 < 0.1%	2.00

Where: D: coefficient referring to the amount of CO_2, K is the coefficient dependent on the relative humidity.

Table 3. Factors for the corresponding cement types used in the CD model.

Cement Type	r_c
Portland cement (PC 40) and (PC 45)	0.80
Portland cement (PC 50) and (PC 55)	1.00
Portland cement +15% mineral addition	1.20
Portland cement +30% mineral addition	1.40
Portland cement +50% mineral addition	2.00

Where: r_c is the coefficient related to cement type.

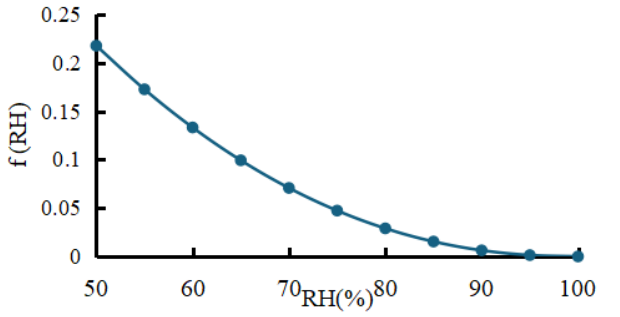

Figure 1. Factors of the relative humidity versus the corresponding different relative humidity levels, where f (RH) is the relative humidity factor.

Kwon and Na[60] stated that the presence of cracks at a specific range in RC sections accelerates the carbonation depth of concrete. The crack width in Equation (5) ranges from 0.10 mm to 0.20 mm. However, Equation (6) allows computing the CD at a specified crack width ranging from 0.05 mm to 0.35 mm according to Al-Ameeri et al.[58]. **Figure 2** shows that the factor of the crack for the Al-Ameeri et al.[58] mathematical model across various crack widths is higher than the Kwon and Na[60] carbonation model, by approximately value of 2.6.

$$f_{c3} = 2.816 \times \sqrt{W_c} + 1 \quad (5)$$

$$f_{c3} = 11.4 \times \sqrt{W_c} + 1 \quad (6)$$

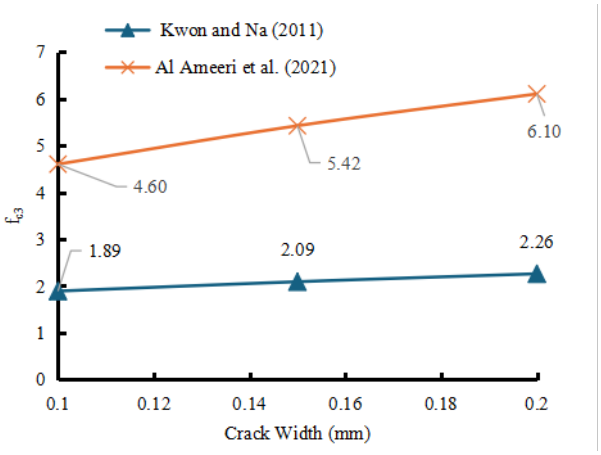

Figure 2. The factor of crack width against different crack widths using two different mathematical models, where f_{c3} is the factor for the impact of cracks with various crack widths on the effective CO_2 diffusion coefficient.

CO_2 concentrations for four emission scenarios: RCPs are based on simulations from five different Earth system models[5]. Projection of atmospheric CO_2 at various emission scenarios[5]. Second-degree polynomial functions are used to calculate the average CO_2 concentrations across various RCPs in the Stewart et al.[44] CD model. These calculations are based on the least squares regression method between various CO_2 concentration scenarios and future years, as shown in **Table 4**. Yoon et al.'s[27] mathematical model assumed CO_2 is constant for all times. It is a point-in-time predictive model. However, Stewart et al.[44] calculated CDs due to enhanced atmospheric CO_2 concentrations using the average CO_2 concentration over time.

Table 4. Relationship between CO_2 concentration over time (Years) at different emission scenarios.

Emission Scenarios	Equations for CO_2 Concentration Used in Stewart's Model
RCP2.6 (Low Emission Scenario)	$CO_2(t) = (-0.0217 \times T^2) + (89.309 \times T) - 91393$ ($R^2 = 0.88$)
RCP4.5 (Intermediate Emission Scenario)	$CO_2(t) = (0.0023 \times T^2) - (6.9314 \times T) + 5081.9$ ($R^2 = 0.97$)
RCP8.5 (High Emission Scenario)	$CO_2(t) = (0.0429 \times T^2) - (169.97 \times T) + 168887$ ($R^2 = 0.99$)

Where CO_2 (t) = average CO_2 concentration over time (PPM); T = time (years), ranging from 2000 to 2100; RCP is the representative concentration pathway.

5. Influences of SCM on Carbonation-Induced Corrosion

Mineral admixtures, also called SCM, act as pozzolanic materials and fine fillers; thereby, the microstructure of the

hardened cement matrix for the uncarbonated zone becomes denser. Supplementary mineral admixtures, such as SF, FA, and SG, are key factors for developing concrete microstructures with high durability and low permeability. It has been found that using mineral admixtures improves the pore structures of concrete.

FA binds calcium hydroxide because of the pozzolanic reaction: this will lead to a decrease in the Ca $(OH)_2$ content in concrete. Some researchers deduced that the presence of FA in concrete mix increases the depth of carbonation (see **Table 5**)[26,64–66]. A considerable decrease in the CD of the concrete was observed by increasing the SF content, as shown in **Table 5**. SF is characterized by having the powder-filling effect in concrete mixes, modifying the inherent nanostructure of the C-S-H, and reducing the porosity of the concrete microstructure.

Table 5. Impact of various SCMs on the CD.

SCM	CD
FA	• Sisomphon and Franke[64] mentioned that increasing the percentage of FA by more than 30% significantly increases the carbonation rate and depth. • Concrete mixes with high-calcium FA are more resistant to carbonation than low-calcium FA mixes, according to Aguayo et al.[65] and Hassan et al.[26]. • Hassan et al.[26] found that for an uncracked concrete cover of 40 mm, the impact of different percentages of either HCFA or LCFA, ranging from 5% to 30% in the concrete mix, has a negligible influence on the PCICI in various years. However, Hassan et al.[26] observed that for the cracked concrete cover of 50 mm with 0.2 mm crack width, the PCICI increased significantly when percentages of LCFA varied from 20% to 30% as SCM in the concrete mixes for the RC member. The impact of HCFA has a low effect on the PCICI compared to LCFA, according to Hassan et al.[26], Aguayo et al.[65], and Khunthongkeaw et al.[66].
SF	• A considerable decrease in the CD of the concrete was observed by increasing the SF content[67]. • Elsalamawy et al.[14] found that the CD decreased by 58% when 10% of SF was added to high-SG cement concrete. Therefore, adding SF to high SG cement concrete improves the concrete's carbonation resistance and its compressive strength.
GGBFS	• The rate of carbonation and CD increased as the percentages of GGBFS used as SCM in concrete mixes increased[29]. In addition, Zhao et al.[29] deduced that the CD for the concrete mix composed of 70% GGBFS increased by 270% compared to the OPC concrete. • Black[30] found that at a low level of SG, around 10% is replaced with the OPC, the pozzolanic reaction reduces the permeability of concrete, thus reducing the penetration of CO_2 into concrete and hindering carbonation.

6. Methods of Prediction of the PCICI

Probabilistic corrosion initiation models, for carbonation-induced corrosion, are necessary to address the uncertainties in predicting deterioration and managing maintenance for the initiation and propagation stages.

The parameters used for two carbonation depth models (Kwon and Na[60] and Al-Ameeri et al.[58]) in their performance functions to predict the PCICI, for the cracked concrete, are defined in **Table 6**. Moreover, the W/C ratio used in the concrete mix is set at 0.4 as defined in **Table 6**. Furthermore, the effective diffusion coefficient for CO_2 considered the impact of relative humidity (RH = 70%) at different percentages and types of FA utilized as SCM in the concrete mixes for the RC decks. **Figure 3** shows the values of the effective diffusion coefficient of CO_2 across various percentages of either high or low calcium FA, which are utilized in the carbonation depth models and the probability of corrosion initiation.

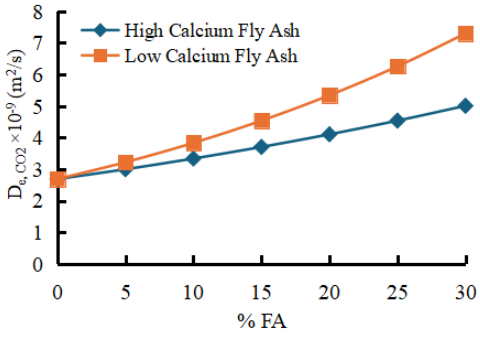

Figure 3. Effective diffusion coefficient for CO_2 versus various percentages of two types of FA used in the concrete mix.

Table 6. Definition of the parameter's value used in the performance function for the carbonation-induced corrosion initiation stage for cracked concrete.

Input Parameter	Value	Distribution
W (kg/m^3)	184	Deterministic
Concrete Cover (CV) (mm)	μ = CV+6, σ = 11.5, according to McGee [68]	Normal Distribution
$D_{e,\,CO2}$ (m^2/s)	(See **Figure 3**)	Deterministic
ρ_c (kg/m^3)	3100 kg/m^3 (COV = 1%)	Normal Distribution, according to Teplý et al. [69]
ρ_w (kg/m^3)	1000 (COV = 1%)	Normal Distribution
Efficiency factor (K)	μ = 0.7 (HCFA) (containing approximately 39.21% SiO_2, 22.78% CaO) according to Papadakis and Tsimas [59] (COV = 10%)	Normal Distribution according to Papadakis and Tsimas [59]
	μ = 0.5 (LCFA) (containing approximately 53.50% SiO_2, 3.38% CaO) according to Papadakis and Tsimas [59] (COV = 10%)	
RH (%)	70%	Deterministic

Where: μ is the statistical mean, COV is the coefficient of variation, W is the weight of water (kg/m^3), ρ_c is the density of cement (kg/m^3), ρ_w is the density of water (kg/m^3).

6.1. Formulation of the Performance Function for the Carbonation-Induced Corrosion Initiation

The performance function for the carbonation-induced corrosion initiation stage can generally be formulated as the difference between a term equivalent to resistance (R) (representing concrete cover (CV)) and a term equivalent to a load effect (L) (representing the carbonation depth $X_c(t)$), as shown in Equations (7) and (8). Failure can be defined as the event when CD exceeds the concrete cover, as shown in Equation (8). **Table 7** shows various latest performance functions for the carbonation-induced corrosion initiation stage for both uncracked and cracked reinforced concrete sections, dealing with the uncertainty for different random variables defined in the performance functions. Performance functions for serviceability are generated to illustrate the various phases associated with damage initiation and accumulation in concrete structures, such as cracking, spalling, and delamination of the concrete.

$$G = R - L \tag{7}$$

$$\begin{cases} G = R - L = 0 & (\text{Limit State}) \\ G = R - L > 0 & (\text{Corrosion doesnt exist}) \\ G = R - L < 0 & (\text{Corrosion exist}) \end{cases} \tag{8}$$

Table 7. Various performance functions for the carbonation-induced corrosion initiation stage at different types of RC sections.

Performance Function	Types of RC Sections	References
$G = CV - \sqrt{\frac{2 \times D_{e,\,CO2} \times \left(\frac{CO_2}{100}\right) \times t}{0.218 \times (C + kP)}}$	Un-cracked Concrete	Hassan et al. [26]
$G = CV - \sqrt{\frac{2\, f_T(t) \times D_{co2}(t)}{a}\, K_{urban} \int_{2000}^{t} C_{co2}\,(t)\, dt}$		Hassan et al. [12,13] & Stewart et al. [44]
$G = CV - X_c\,(t) = \sqrt{\frac{2\, D_{co2}(t)}{a}\, K_{urban}\; C_{co2}\,(t - 1999)}$		Hassan et al . [13], Yoon et al. [27] & Stewart et al. [44]
$G = CV - \left(\sqrt{\frac{2 \times D_{e,\,CO2} \times \left(\frac{CO_2}{100}\right) \times t}{0.218 \times (C + kP)}} \times (2.816 \times \sqrt{W_c} + 1)\right)$	Cracked Concrete	Hassan et al. [26]
$G = CV - \left(\sqrt{\frac{2 \times D_{e,\,CO2} \times \left(\frac{CO_2}{100}\right) \times t}{0.218 \times (C + kP)}} \times (11.4 \times \sqrt{W_c} + 1)\right)$		Al-Ameeri et al. [58]

Where CV = concrete cover for the RC deck, and G = performance function for the carbonation-induced corrosion initiation stage.

Reliability is defined as the probability of a performance function G(X) greater than zero or the probability that the random variables are in the safe region. However, the probability of failure is defined as the probability that the random variables are in the failure region or the performance function by G(X) is less than zero. Reliability is computed as shown in Equation (9).

$$R = 1 - p_f = P\{G(X) > 0\} = \int_{G(x) > 0} f_x(X) \quad dx \quad (9)$$

Calculating the probability of failure (P_f) can be easily done using the standard normal cumulative function, as illustrated in Equation (9). For a normal distribution of the performance function (G(X)) values, the P_f is computed explicitly to the reliability index (β) value as illustrated in Equation (10).

$$P_f = \Phi(-\beta) = 1 - \Phi(\beta) \quad (10)$$

6.2. Different Methods for Predicting the PCICI

6.2.1. The Montecarlo Simulation (MCS) Method

The P_f can be calculated using several methods. The most obvious and straightforward way to conduct the P_f is the MCS method. It consists of simulating outcomes of the performance function and counting the number of failure events obtained. This method attempts to characterize the whole failure domain, so it needs an essential number of simulations.

Many researchers developed several methodologies to calculate the P_f[12,13,15,16,26]. Crude MCS method[70,71], First and Second Order Reliability Methods (FORM and SORM)[72] are among such reliable techniques. Based on the Monte Carlo simulation approach, the probability of failure is calculated as shown in Equation (11) if the number of design points (N_{MCS}) is sufficiently large. Despite the high accuracy that can be achieved using the MCS method, the required significantly large number of simulations of the performance function presents a significant challenge for many applications where system performance evaluation is costly. Advanced methods use a more efficient way to select simulations based on two main concepts: first, the approximation of the nonlinear state function, and second, the efficient method of simulations.

$$P_f^{MCS} = \frac{N_{G(x)<0}}{N_{MCS}} \quad (11)$$

Where $N_{G(x)}$ = number of design points that satisfy $G(x) < 0$ out of the total number of simulations (N_{MCS}).

6.2.2. The First-Order Reliability Method (FORM)

The FORM expresses the probability of failure as a function of the reliability index. Using mathematical techniques, the multiple integrals of P_f can be reduced to a simple integral. Therefore, the probability of corrosion is evaluated as in Equation (12).

$$P_f = \int_{h(u1,\ u2)} f_{(U_1 U_2)}(u_1 u_2)\, du_1 du_2 = \frac{1}{\sqrt{2\pi}} \int_{-\infty}^{-\beta} e^{\frac{-u_1^2}{2}}\, du_1 = \varnothing(-\beta) \quad (12)$$

The input variables are transformed into multinormal Gaussian variables with symmetry around the mean value point, representing the U space's origin. The design point (P^*) is a point in the failure domain that is the closest to the origin. The distance (OP^*) separating it from the origin is called the Hasofer–Lind reliability index (β_{HL})[73]. This index is determined by solving the following nonlinear optimization problem as follows:

$$\beta_{HL} = \min \sqrt{\sum\nolimits_i u_i^2} \quad (13)$$

Subject to $h(u_1, u_2) \leq 0$

where $h(u_1, u_2)$ is the transformed limit state function in the standard space.

$$P_{f,FORM} = \varnothing(-\beta) = 1 - \varnothing(\beta) \quad (14)$$

Where $\varnothing(.)$ is the cumulative distribution function of the normal distribution, the probability of failure is calculated using FORM, as discussed in Equation (14).

6.2.3. The Second-Order Reliability Method (SORM)

The SORM uses the second-order Taylor expansion to approximate the performance function at the MPP (u*) as shown in Equation (15).

$$g(U) \approx q(U) = g(u^*) + \nabla(u^*) \times (U - u^*)^T + \tfrac{1}{2} \times (U - u^*) \times H(u^*) \times (U - u^*)^T \quad (15)$$

where H (u*) is the Hessian matrix at the MPP.

The probability of failure can be calculated, as shown in Equation (16), when β It is large enough.

$$p_f = P\{g(X) < 0\} = \varnothing(-\beta) \prod_{i=1}^{n-1} (1 + \beta\, k_i)^{\frac{1}{2}} \qquad (16)$$

Where k_i represents the i^{th} main curvature of the performance function g(U) at the most probable point.

6.2.4. The Advanced First-Order Reliability Method (Hasofer-Lind Method)

This method is an advanced version of FORM. Moreover, this method transforms the variables into a standardized space. Standard normal variables have a zero mean and a unit standard deviation of 1. This coordinate space transformation is performed to aid in the computation of the reliability index. A random variable (x_i) is reduced, as shown in Equation (17). Each random variable in the performance function is substituted by the respective reduced equations, and the corresponding performance function is obtained. The reduced coordinate system's limit state surface is called g(X') = 0.

$$X_i' = \frac{x_i - \mu_{x_i}}{\sigma_{x_i}} \qquad (i = 1,\ 2,\ \cdots,\ n) \qquad (17)$$

Where: X_i' is a random variable characterized by a probability density function with zero mean and unit standard deviation.

The Hasofer-Lind reliability index (β_{HL}) is the minimum distance between the origin and the limit state surface. Thus, the determination of this point has a main important aspect: the optimization of the distance to find the minimum distance point, with the constraint that the point lies on the limit state surface. This minimum distance lies on the limit state surface (i.e., design point (x'*)). Therefore, the Hasofer–Lind reliability index is written in Equation (18).

$$\begin{cases} Minimize\ D = \sqrt{(X'^*)^T \times X'^*} \\ Subjecting\ to\ constraint\ g\left(X'\right) = 0 \end{cases}$$

$$\beta_{HL} = \sqrt{(X'^*)^T \times X'^*} \qquad (18)$$

Finally, the probability of failure is calculated from the reliability index, as illustrated in Equation (19).

$$P_f = \Phi(-\beta_{HL}) \qquad (19)$$

7. Analysis of Results

7.1. Projection of the CD across Various Crack Widths Using the Al-Ameeri Mathematical Model

The CO_2 concentration in the CD model was set at 940 PPM, which corresponds to the projection of CO_2 concentration in the year 2100, the worst emission scenario according to IPCC[5]. The CD was conducted using the Al-Ameeri et al.[58] mathematical model for cracked concrete. The total amount of cement used in the concrete mix for the RC deck is 460 kg/m^3. **Figure 4** shows the projection of the CD across various crack widths at various percentages and types of FA; the CD values increased from 44.8 mm to 97.8 mm when the crack width changed from 0.05 mm to 0.35 mm, respectively, especially at 0% for both the LCFA and HCFA. For a 30% LCFA used as SCM in the concrete mix for the RC deck, it was deduced that the CD value increased sharply from 80 to 174.5 mm when the crack width changed from 0.05 mm to 0.35 mm, as shown in **Figure 4a**. **Figure 4b** shows that the CD also increased from 64 mm to 139.7 mm for concrete mixes, including 30% of HCFA, when the crack width for the RC deck changed from 0.05 mm to 0.35 mm, respectively. **Table 8** shows that the relationship between the projected CD conducted using the Al-Ameeri et al.[58] mathematical model and various crack width ranges for cracked concrete is a second-degree polynomial function, for RC decks made of various percentages and types of FA, subjected to a CO_2 concentration of 940 PPM at the age of 100 years of CO_2 exposure.

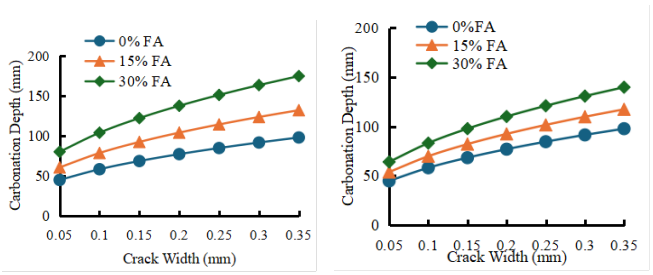

(a) **(b)**

Figure 4. CD value corresponding to different crack widths for RC members, including various percentages and types of FA as SCM in concrete mixes, (**a**) LCFA; (**b**) HCFA.

Table 8. Polynomial functions for predicting the CD for the cracked RC member subjected to 940 PPM as a function of various ranges of crack widths at different percentages and types of FA at T = 100 years.

Percentages of FA	LCFA	HCFA
0%	$CD = (-256.98 \times CW^2) + (275.6 \times CW) + 32.373$ ($R^2 = 0.99$)	$CD = (-256.54 \times CW^2) + (275.13 \times CW) + 32.319$ ($R^2 = 0.99$)
15%	$CD = (-346.45 \times CW^2) + (371.56 \times CW) + 43.645$ ($R^2 = 0.99$)	$CD = (-308.12 \times CW^2) + (330.45 \times CW) + 38.816$ ($R^2 = 0.99$)
30%	$CD = (-458.23 \times CW^2) + (491.44 \times CW) + 57.726$ ($R^2 = 0.99$)	$CD = (-366.9 \times CW^2) + (393.49 \times CW) + 46.221$ ($R^2 = 0.99$)

where CD = carbonation depth (mm); and CW = crack width ranging from 0.05 mm to 0.35 mm.

7.2. Projection of the CD across Various CO_2 Concentrations Using the Al-Ameeri Model for Cracked Concrete

The CDs were conducted using Al-Ameeri et al. [58] and Kwon and Na [60] mathematical models for cracked concrete having a crack width of 0.2 mm across various CO_2 concentrations ranging from 200 PPM to 1400 PPM in the year 100, as shown in **Figure 5** and **Figure 6**, respectively. The CD values conducted using Al-Ameeri et al. [58] are higher than the CD values conducted using Kwon and Na [60] by a factor of 2.69 across various CO_2 concentrations ranging from 200 to 1400 PPM, as shown in **Figures 5 and 6**. It was found that the relationship between CO_2 concentrations ranging from 200 to 1400 PPM and the corresponding CD values is a second-degree polynomial function at various percentages of 15% or 30% of either high or LCFA used in the mix for RC members, as shown in **Figures 5** and **6**, and **Table 9**.

Table 9. Polynomial functions for predicting the CD for the cracked RC member with a crack width of 0.2 mm as a function of various ranges of CO_2 concentrations at different percentages of FAs at T = 100 years.

Percentage of FA	CD Models	
	Al-Ameeri et al. [58]	Kwon and Na [60]
15% LCFA	$CD = (-2 \times 10^{-5} \times CO_2^2) + (0.1025 \times CO_2) + 29.364$ ($R^2 = 0.99$)	$CD = (-9 \times 10^{-6} \times CO_2^2) + (0.038 \times CO_2) + 10.88$ ($R^2 = 0.99$)
15% HCFA	$CD = (-2 \times 10^{-5} \times CO_2^2) + (0.0912 \times CO_2) + 26.115$ ($R^2 = 0.99$)	$CD = (-8 \times 10^{-6} \times CO_2^2) + (0.0338 \times CO_2) + 9.6759$ ($R^2 = 0.99$)
30% LCFA	$CD = (-3 \times 10^{-5} \times CO_2^2) + (0.1356 \times CO_2) + 38.838$ ($R^2 = 0.99$)	$CD = (-1 \times 10^{-5} \times CO_2^2) + (0.0502 \times CO_2) + 14.39$ ($R^2 = 0.99$)
30% HCFA	$CD = (-3 \times 10^{-5} \times CO_2^2) + (0.1085 \times CO_2) + 31.097$ ($R^2 = 0.99$)	$CD = (-9 \times 10^{-6} \times CO_2^2) + (0.0402 \times CO_2) + 11.522$ ($R^2 = 0.99$)

Where CO_2 concentration ranges from 200 PPM to 1400 PPM.

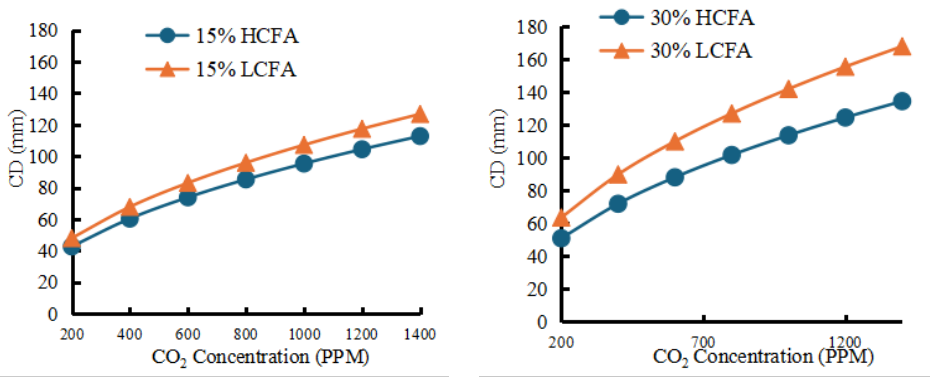

(**a**) (**b**)

Figure 5. Projection of the CD values across various CO_2 concentrations using the Al-Ameeri mathematical model for cracked concrete with a crack width of 0.2 mm at T = 100 years, (**a**) 15% SCM; (**b**) 30% SCM.

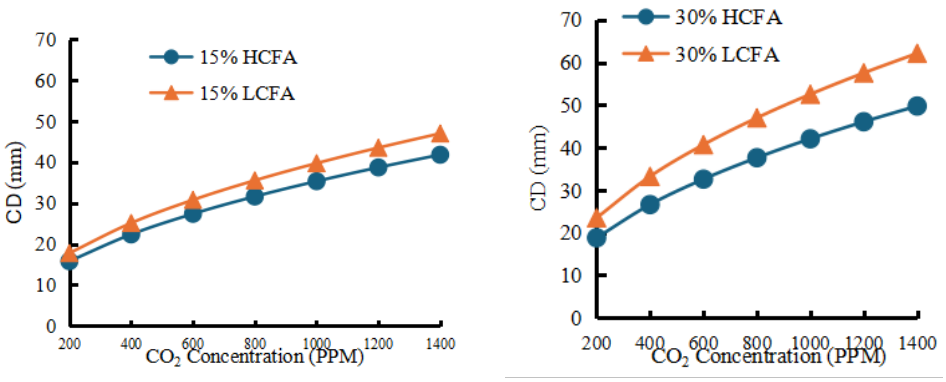

(**a**) (**b**)

Figure 6. The CD values were projected across various CO_2 concentrations using Kwon and Na[60], a carbonation model for cracked concrete with a crack width of 0.2 mm at 100 years of CO_2 exposure, (**a**) 15% SCM; (**b**) 30% SCM.

The CD values were determined using Papadakis and Tsimas[59] for uncracked concrete across various CO_2 concentrations, ranging from 200 to 1400 PPM, for concrete mixes with different percentages and types of FA, as shown in **Figure 7**. It was deduced that the relationship between CO_2 concentrations ranging from 200 to 1400 PPM and the corresponding CD values is a second-degree polynomial function at various percentages of either HCFA or LCFA used in the mix for RC sections, as shown in **Figure 7** and **Table 10**.

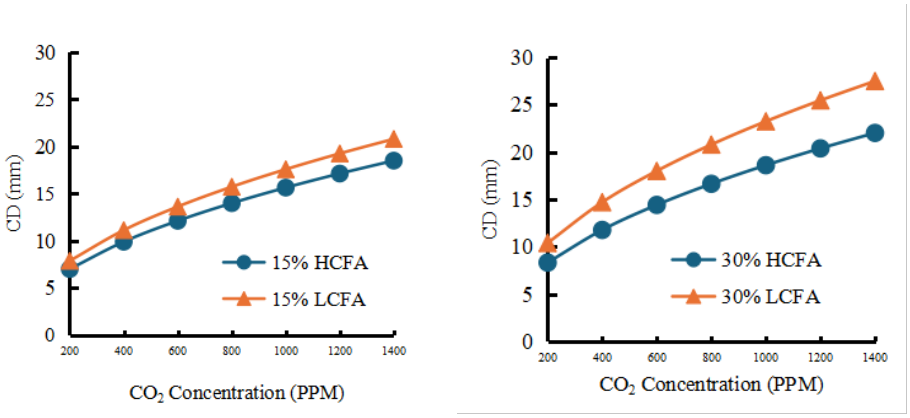

(**a**) (**b**)

Figure 7. Projection of the CD values across various CO_2 concentrations for uncracked concrete consisting of various percentages and types of FA, (**a**) 15% SCM; (**b**) 30% SCM.

Table 10. Polynomial functions for predicting the CD values using Papadakis and Tsimas's[59] model for the uncracked RC member, as a function of various ranges of CO_2 concentrations at different percentages of FA at 100 years of CO_2 exposure.

Percentage and Types of FA	Uncracked Concrete Section
15% LCFA	$CD = (-4\times10^{-6} \times CO_2^2) + (0.0168 \times CO_2) + 4.8153$ ($R^2 = 0.99$)
15% HCFA	$CD = (-3\times10^{-6} \times CO_2^2) + (0.0149 \times CO_2) + 4.2826$ ($R^2 = 0.99$)
30% LCFA	$CD = (-5\times10^{-6} \times CO_2^2) + (0.0222 \times CO_2) + 6.369$ ($R^2 = 0.99$)
30% HCFA	$CD = (-4\times10^{-6} \times CO_2^2) + (0.0178 \times CO_2) + 5.0996$ ($R^2 = 0.99$)

7.3. Comparison of CD Values between Al-Ameeri and Kwon and Na Mathematical Models for Cracked Concrete

The CO_2 concentration applied to the RC member is assumed to equal 940 PPM to conduct the CD values in year 100 across various percentages of either HCFA or LCFA, ranging from 5% to 30%, using Al-Ameeri et al.[58] and Kwon and Na[60] as shown in **Figure 8**. The CDs for cracked concrete having a crack width of 0.2 mm, conducted using Al-Ameeri et al.[58] across various percentages of either HCFA or LCFA, are higher than those performed using the Kwon and Na[60] mathematical model by a factor of 2.7, as shown in **Figure 8**.

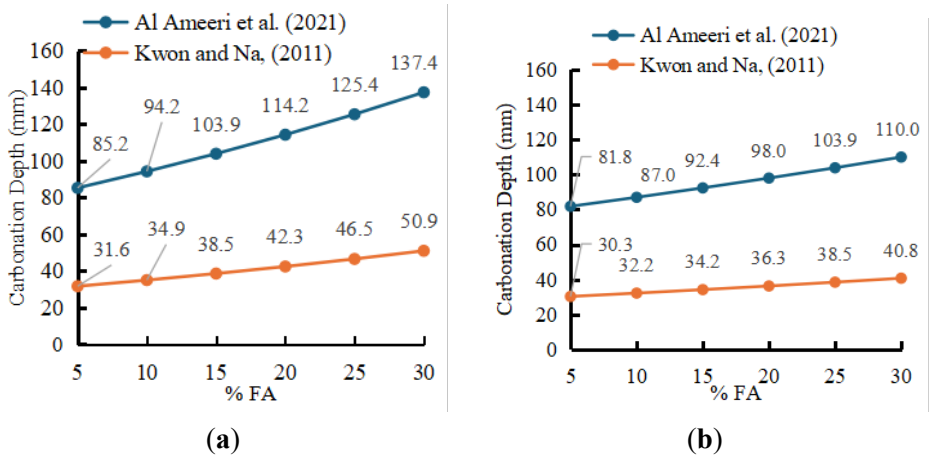

Figure 8. Projection of the CD values across various percentages and FA types for cracked concrete with a crack width of 0.2 mm, (**a**) LCFA; (**b**) HCFA.

The concentration of CO_2 applied to the RC member is assumed to be equal to 940 PPM to conduct the CD values in year 100 across various percentages of either HCFA or LCFA, ranging from 5% to 30%, using the mathematical model as shown in **Figure 9**. The CDs for uncracked concrete conducted across various percentages of LCFA and HCFA change slightly from (14 mm to 22.5 mm) and from (13.4 mm to 18 mm), respectively, when the percentages of FA change from 5% to 30%, as shown in **Figure 9**.

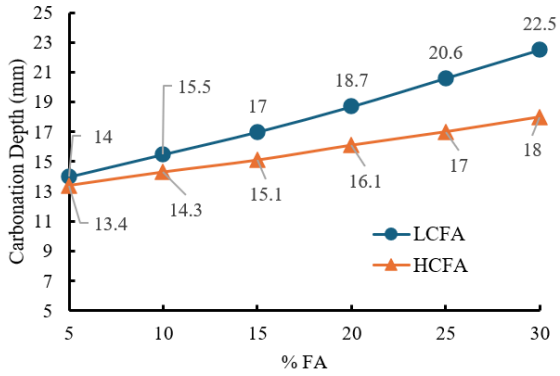

Figure 9. The CD values are projected across various percentages of FA for uncracked concrete, consisting of various percentages and types of FA.

The CD values for cracked concrete having a crack width of 0.2 mm conducted using Kwon and Na[60] are higher than the uncracked concrete by a factor of approximately 2.26 across various percentages of either HCFA or LCFA ranging from 5% to 30% utilized as a partial replacement with the amount of cement used in mixes for RC sections (see **Tables 11** and **12**). However, the CD values for cracked concrete conducted using Al-Ameeri et al.[58] are higher than those of uncracked concrete by a significant factor of 6.10 across various percentages of either HCFA or LCFA, ranging from 5% to 30% utilized as SCM, with the amount of cement used in mixes for RC sections as shown in **Tables 11** and **12**.

7.4. Investigation of the PCICI across Various Types and Percentages of FA Using Kwon and Na and Al-Ameeri Mathematical Models for Cracked Concrete

The probabilistic carbonation-induced corrosion models have been validated across different percentages and types of FA and compared with the results obtained by several researchers, Teplý et al.[69], and Hassan et al.[26]. The results

of the recent model align with those obtained by Teplý et al.[69] and Hassan et al.[26]. The probabilistic model used in this research demonstrated its robustness and accuracy in predicting the PCICI.

Table 11. Projection of the CD for uncracked and cracked concrete across various percentages of HCFA used in the concrete mixes for RC members.

Types of RC Member Sections	% HCFA					
	5%	10%	15%	20%	25%	30%
Cracked Concrete Kwon and Na[60]	30.30	32.20	34.20	36.30	38.50	40.80
Cracked Concrete Alameeri et al.[58]	81.80	87	92.40	98	103.90	110
Uncracked Concrete	13.40	14.30	15.10	16.10	17	18
Factor[1]	2.26	2.25	2.26	2.25	2.26	2.27
Factor[2]	6.10	6.10	6.11	6.10	6.11	6.11

Table 12. Projection of the CD for uncracked and cracked concrete across various percentages of LCFA used in the concrete mixes for RC members.

Types of RC Member Sections	% LCFA					
	5%	10%	15%	20%	25%	30%
Cracked Concrete Kwon and Na[60]	31.60	34.90	38.50	42.30	46.50	50.90
Cracked Concrete Al-Ameeri et al.[58]	85.20	94.20	103.90	114.20	125.40	137.40
Uncracked Concrete	14	15.50	17	18.70	20.60	22.50
Factor[1]	2.26	2.25	2.26	2.26	2.26	2.26
Factor[2]	6.10	6.10	6.11	6.11	6.10	6.11

where Factor[1] = $\frac{CD\ for\ cracked\ concrete\ conducted\ using\ Kwon\ and\ Na\ [59]}{CD\ for\ Uncracked\ concrete}$,

Factor[2] = $\frac{CD\ for\ cracked\ concrete\ conducted\ using\ Al\ Ameeri\ et\ al.\ [60]}{CD\ for\ Uncracked\ concrete}$

The cracked RC decks utilized in the probabilistic models[59,60] have a concrete cover of 70 mm, subjected to the impact of CO_2 at 1000 parts per million, after 100 years of CO_2 exposure. The performance function for cracked concrete was developed using the Al-Ameeri et al.[58] model to investigate the PCICI values across various percentages of either LCFA or HCFA at different crack widths, as shown in **Figure 10**. The parameters utilized in the probabilistic model deal with the uncertainty, as mentioned in **Table 6**. The PCICI was conducted using the MCS method, with 100,000 simulations for each random variable that dealt with uncertainty. It was observed that the PCICI changed sharply from 2% to 71% and from 20% to 100%, when the percentages of LCFA increased from 5% to 30% utilized as SCM in concrete mixes for cracked RC decks having a crack width of 0.05 mm and 0.1 mm, respectively, as shown in **Figure 10a**. The change of the HCFA from 5% to 30% used in the mixes for cracked RC decks with crack widths of 0.05 mm and 0.1 mm led to a significant increase in the PCICI from 1% to 19% and from 14% to 80%, respectively, as shown in **Figure 10b**. Crack width of 0.1 mm in the RC decks would lead to a significant impact on the PCICI compared to 0.05 mm, when the percentage of LCFA varies from 5% to 30% as SCM. Finally, it was deduced that the impact of the HCFA, ranging from 5% to 15% used as SCM in the mixes for cracked RC decks with crack widths of 0.05 mm, led to a negligible effect on the PCICI, as shown in **Figure 10b**. Therefore, it is recommended to limit the amount of HCFA in the mixes that are subjected to severe CO_2 concentration of 1000 parts per million in the future to a percentage below 15% for a cracked RC deck with a width of 0.05 mm. Furthermore, it is recommended to use HCFA at lower percentages in the concrete mix instead of LCAF to enhance the durability of RC structures.

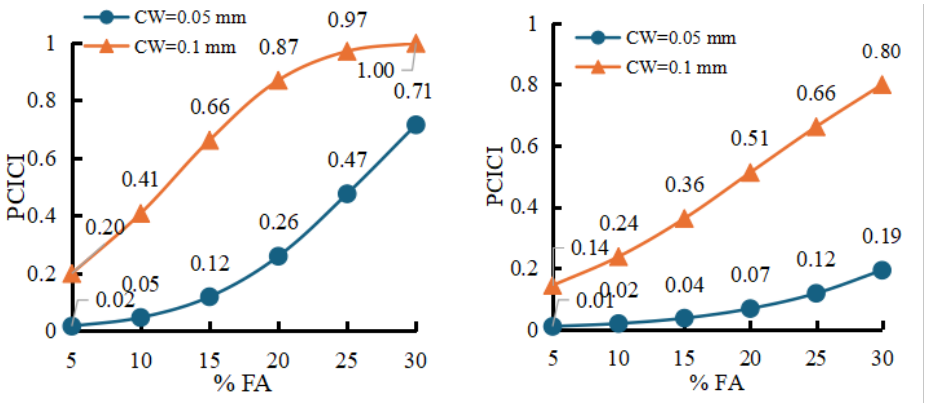

(**a**) (**b**)

Figure 10. Influence of various percentages and types of FA on the PCICI for cracked RC decks having various crack widths at the age of 100 years of CO_2 exposure, (**a**) LCFA; (**b**) HCFA.

The performance function for cracked concrete was developed using Kwon and Na[60] mathematical model to assess the PCICI values across various percentages of LCFA and HCFA at different crack widths (see **Figure 11**). The impact of the LCFA, ranging from 5% to 15% used in the mixes for cracked RC decks with crack widths of either 0.05 mm or 0.1 mm, led to zero values in the PCICI values, as shown in **Figure 11a**. Moreover, the impact of 15% to 30% LCFA utilized as SCM in the mixes for cracked RC decks with crack widths of either 0.05 mm or 0.10 mm has a very low impact on the PCICI compared to the PCICI obtained from the Al-Ameeri et al.[58] model (see **Figure 11a**). The influence of the HCFA, ranging from 5% to 30% utilized in the mixes for cracked RC decks with crack widths of either 0.05 mm or 0.1 mm, led to approximately zero values in the PCICI values, as shown in **Figure 11b**. Finally, the impact of various crack widths, including (0.05 mm or 0.1 mm), is negligible on the PCICI across different percentages ranging from 5% to 30% of either HCFA or LCFA used as SCM in the mix for RC deck having a mean concrete cover of 70mm.

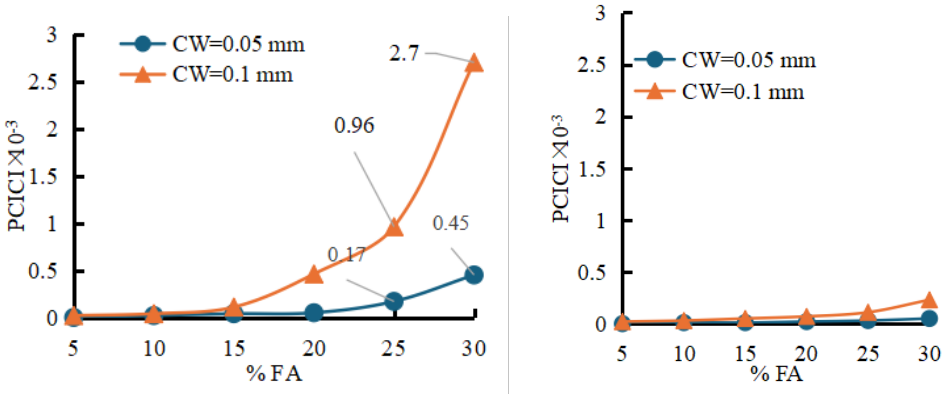

(**a**) (**b**)

Figure 11. Impact of different percentages and types of FA on the PCICI for the RC decks with various crack widths at T = 100 years of CO_2 exposure, (**a**) LCFA; (**b**) HCFA.

8. Conclusions

- The relationship between the projected CD calculated via the Al-Ameeri mathematical model and various crack width ranges from 0.05 mm to 0.35 mm is a second-degree polynomial function, for cracked RC decks subjected to a CO_2 concentration of 940 PPM at 100 years of CO_2 exposure, which is made of various percentages of both HCFA and LCFA. Moreover, the relationship between CO_2 concentrations ranging from

200 to 1400 PPM and the corresponding CD values, conducted using either Kwon and Na [60] or Al-Ameeri et al. [58] mathematical models, is a second-degree polynomial function across various percentages and types of FA utilized in the mix for cracked RC members, with a crack width of 0.2 mm.

- CD values for cracked concrete with a crack width of 0.2 mm, conducted via the Kwon and Na model, are higher than the CD for uncracked concrete by a factor of 2.26 across different percentages ranging from 5% to 30% of either HCFA or LCFA utilized as a SCM, with the amount of cement used in mixes for RC decks. However, the projected CD values for cracked concrete using Al-Ameeri et al. [58] are higher than those of uncracked concrete by a significant factor of 6.10 across various percentages varying from 5% to 30% of either HCFA or LCFA utilized as SCM in mixes for RC decks.
- Crack width of 0.1 mm in the RC decks would lead to a severe impact on the PCICI conducted using the Al-Ameeri et al. [58] model compared to the Kwon and Na [60] model, when the percentage of LCFA varies from 5% to 30% as SCM.
- The impact of various crack widths, for either 0.05 mm or 0.1 mm, had a negligible impact on the PCICI calculated using the Kwon and Na [60] model across various percentages of either HCFA or LCFA, ranging from 5% to 30% as SCM in the mixes for RC decks with a mean concrete cover of 70mm.
- The impact of the HCFA, ranging from 5% to 15% in the mixes for cracked RC decks with crack widths of 0.05 mm, would lead to a negligible influence on the PCICI obtained from the Al-Ameeri et al. [58] mathematical model.

Limitations

In this research, the CO_2 concentration is assumed to be equal to 1000 ppm as the worst emission scenario (RCP8.5), which corresponds to the projection of the CO_2 concentration conducted by IPCC (2014) in the year 2100. The mean concrete cover used in the probabilistic model is assumed to be equal to 70 mm, dealing with the uncertainty. Moreover, the relative humidity utilized in most of the carbonation depth models and the probability of corrosion is assumed to be equal to 70%. Furthermore, the W/C ratio used in the concrete mix is set at 0.4, and the total amount of cement utilized in the concrete mix is set at 460 kg/m^3. The crack widths utilized in the probabilistic models are assumed to be equal to 0.05 mm and 0.1 mm in the performance functions.

It is recommended to mitigate the amount of HCFA in the mixes for cracked RC decks with a width of 0.05 mm, which are subjected to a severe CO_2 concentration of 1000 parts per million, to a percentage below 15% to inhibit carbonation-induced corrosion initiation. Moreover, it is also recommended to use HCFA at lower percentages in the mix instead of LCAF to enhance the durability and serviceability of RC structures. In the future, it is suggested to predict the carbonation depth across different fly ash percentages using computer vision and deep learning, which involves robust and efficient vision-based models according to Kabir et al. [74] and Song et al. [75].

Funding

This work received no external funding.

Institutional Review Board Statement

Not applicable.

Informed Consent Statement

Not applicable.

Data Availability Statement

The data used in this study are available from the corresponding author upon reasonable request.

Conflicts of Interest

The author declares no conflict of interest.

References

[1] Pang, L., Li, Q., 2016. Service life prediction of RC structures in the marine environment using long-term chloride ingress data, comparison between exposure trials and real structure surveys. Construction and Building Materials. 113, 979–987. DOI: https://doi.org/10.1016/j.conbuildmat.2016.03.156

[2] Croce, P., Formichi, P., Landi, F., 2019. Structural safety and design under climate change. In Proceedings of the IABSE Congress, New York: The Evolving Metropolis, New York, NY, USA, 4–6 September 2019.

[3] Bretti, G., Ceseri, M., 2023. Climate Change Effects on Carbonation Process: A Scenario-Based Study. Heritage. 6, 236–257. DOI: https://doi.org/10.3390/heritage6010012

[4] Aminzadegan, S., Shahriari, M., Mehranfar, F., et al., 2022. Factors affecting the emission of pollutants in different types of transportation: A literature review. Energy Reports. 8, 2508–2529. DOI: https://doi.org/10.1016/j.egyr.2022.01.161

[5] IPCC, 2014. Climate Change 2014: Synthesis Report, Contribution of Working Groups I, II, and III to the Fifth Assessment Report of the Intergovernmental Panel on Climate Change. Core Writing Team, Pachauri, R.K., Meyer, L. (Eds.). IPCC: Geneva, Switzerland. Available from: https://epic.awi.de/id/eprint/37530/1/IPCC_AR5_SYR_Final.pdf (cited 15 March 2025).

[6] Bush, E., Lemmen, D.S. (Eds), 2019. Canada's Changing Climate Report. Government of Canada: Ottawa, ON, Canada.

[7] Alhede, A., Dijkstra, J., Robuschi, S., et al., 2020. A two-stage study of steel corrosion and internal cracking revealed by multimodal tomography. Construction and Building Materials. 394, 132187. DOI: https://doi.org/10.1016/j.conbuildmat.2023.132187

[8] Syll, A.S., Kanakubo, T., 2022. Impact of Corrosion on the Bond Strength between Concrete and Rebar: A Systematic Review. Materials. 15, 7016. DOI: https://doi.org/10.3390/ma15197016

[9] Lin, Y., Zhong, S., Yu, G., et al., 2024. Effect of corrosion on bond slipping between steel and concrete in SRC structures. Journal of Constructional Steel Research. 220, 108857. DOI: https://doi.org/10.1016/j.jcsr.2024.108857

[10] Al Fuhaid, A.F., Niaz, A., 2022. Carbonation and Corrosion Problems in Reinforced Concrete Structures. Buildings. 12(5), 586. DOI: https://doi.org/10.3390/buildings12050586

[11] Tongaria, K., Mandal, S., Mohan, D., 2018. A Review on Carbonation of Concrete and Its Prediction Modelling. Journal of Environmental Nanotechnology. 7(4), 76–91. Available from: https://nanoient.org/journals/index.php/jent/article/view/750

[12] Hassan, M., Amleh, L., 2024. Influence of Climate Change on Probability of Carbonation-Induced Corrosion Initiation. Periodica Polytechnica Civil Engineering. 68(1), 57–67. DOI: https://doi.org/10.3311/PPci.22101

[13] Hassan, M., Amleh, L., Othman, H., 2022. Effect of Different Cement Content and Water-Cement Ratio on Carbonation Depth and Probability of Carbonation-Induced Corrosion for Concrete. Cement Wapno Beton. 27, 126–143. DOI: https://doi.org/10.32047/cwb.2022.27.2.4

[14] Elsalamawy, M., Mohamed, A.R., Kamal, E.M., 2019. The role of relative humidity and cement type on carbonation resistance of concrete. Alexandria Engineering Journal. 58(4), 1257–1264. DOI: https://doi.org/10.1016/j.aej.2019.10.008

[15] Amleh, L., Hassan, M., Hussein, L., 2024. Influence of Climate Change on the Probability of Chloride-Induced Corrosion Initiation for RC Bridge Decks Made of Geopolymer Concrete. Sustainability. 16(18), 8200. DOI: https://doi.org/10.3390/su16188200

[16] Hassan, M., Amleh, L., 2025. Influence of Various Crack Widths in RC Bridge Decks on the Initiation of Chloride-Induced Corrosion. Journal of Composites Science. 9(5), 242. DOI: https://doi.org/10.3390/jcs9050242

[17] Schultheiß, A.L., Patel, R.A., Vogel, M., et al., 2023. Comparative Analysis of Engineering Carbonation Model Extensions to Account for Pre-Existing Cracks. Materials. 16(18), 6177. DOI: https://doi.org/10.3390/ma16186177

[18] Forsdyke, J.C., Lees, J.M., 2025. Influence of crack width on carbonation depths in functionally layered concrete. Materials and Structures. 58, 130. DOI: https://doi.org/10.1617/s11527-025-02643-8

[19] Varzina, A., Phung, Q.T., Perko, J., et al., 2022. Synergistic Effects between Carbonation and Cracks in the Hardened Cement Paste. Sustainability. 14(14), 8572. DOI: https://doi.org/10.3390/su14148572

[20] Abd El-Fattah, H., Abd El-Zaher, Y., Kohail, M., 2024. A study of chloride binding capacity of concrete containing supplementary cementitious materials. Scientific Reports. 14, 12970. DOI: https://doi.org/10.1038/s41598-024-62778-6

[21] Jedidi, M., 2024. Carbonation of Concrete: Measurement and Repair. Civil Engineering and Architecture. 12(5), 3664–3674. DOI: https://doi.org/10.13189/cea.2024.120538

[22] Jedidi, M., Belhassen, A., 2020. Carbonation of Reinforced Concrete Structures. Current Trends in Civil and Structural Engineering. 5(2). DOI: https://doi.org/10.33552/CTCSE.2020.05.000609

[23] Mahmood, M., Khan, A.R., Ayub, T., 2022. Carbonation Resistance in Ordinary Portland Cement Concrete with and without Recycled Coarse Aggregate in Natural and Simulated Environment. Sustainability. 14(1). DOI: https://doi.org/10.3390/su14010437

[24] Gu, H., Li, Q., 2022. Updating deterioration models of reinforced concrete structures in carbonation environment using in-situ inspection data. Structure and Infrastructure Engineering. 18(2), 266–277. DOI: https://doi.org/10.1080/15732479.2020.1841246

[25] Anstice, D.J., Page, C. L., Page, M.M., 2005. The

pore solution phase of carbonated cement pastes. Cement and Concrete Research. 35(2), 377–383. DOI: https://doi.org/10.1016/j.cemconres.2004.06.041

[26] Hassan, M., Amleh, L., Hussein, L., 2024. Projection of the Carbonation Depths and its Probability of Corrosion Initiation for the Uncracked and Cracked Concrete. International Review in Civil Engineering (IRECE). 15, 381–398. DOI: https://doi.org/10.15866/irece.v15i5.24986

[27] Yoon, I.-S., Çopuroğlu, O., Park, K.-B., 2007. Effect of global climatic change on carbonation progress of concrete. Atmospheric Environment. 41(34), 7274–7285. DOI: https://doi.org/10.1016/j.atmosenv.2007.05.028

[28] Stewart, M.G., Wang, X., Nguyen, M.N., 2011. Climate change impact and risks of concrete infrastructure deterioration. Engineering Structures. 33(4), 1326–1337. DOI: https://doi.org/10.1016/j.engstruct.2011.01.010

[29] Zhao, J., Shumuye, E.D., Wang, Z., 2021. Effect of Slag Cement on Concrete Resistance Against Combined Exposure To Freeze-Thaw and Chloride Ingress. Journal of Engineering Science and Technology. 16(6), 4687–4706.

[30] Black, L., 2016. Low Clinker Cement as a Sustainable Construction Material. In: Sustainability of Construction Materials, 2nd ed. Elsevier: Amsterdam, Netherlands. pp. 415–457. DOI: https://doi.org/10.1016/B978-0-08-100370-1.00017-2

[31] Gjorv, O.E., 1995. Effect of condensed silica fume on steel corrosion in concrete. ACI Material Journal. 92(6), 591–598. DOI: https://doi.org/10.14359/9778

[32] Qiu, Q., 2020. A state-of-the-art review on the carbonation process in cementitious materials: Fundamentals and characterization techniques. Construction and Building Materials. 247, 118503. DOI: https://doi.org/10.1016/j.conbuildmat.2020.118503

[33] Hargis, C.W., Lothenbach, B., Müller, C.J., et al., 2017. Carbonation of calcium sulfoaluminate mortars. Cement and Concrete Composites. 80, 123–134. DOI: https://doi.org/10.1016/j.cemconcomp.2017.03.003

[34] Lee, H.J., Kim, D.G., Lee, J.-H., et al., 2012. A study for carbonation degree on concrete using a phenolphthalein indicator and Fourier-Transform Infrared Spectroscopy. International Journal of Civil and Environmental Engineering. 6(2), 95–101.

[35] Li, Z., Li, S., 2020. Effects of wetting and drying on alkalinity and strength of fly ash/slag-activated materials. Construction and Building Materials. 254, 119069. DOI: https://doi.org/10.1016/j.conbuildmat.2020.119069

[36] Wang, X., Yang, Q., Peng, X., et al., 2024. A Review of Concrete Carbonation Depth Evaluation Models. Coatings. 14(4), 386. DOI: https://doi.org/10.3390/coatings14040386

[37] Tang, J., Wu, J., Zou, Z., et al., 2018. Influence of axial loading and carbonation age on the carbonation resistance of recycled aggregate concrete. Construction and Building Materials. 173, 707–717. DOI: https://doi.org/10.1016/j.conbuildmat.2018.03.269

[38] Steiner, S., Lothenbach, B., Proske, T., et al., 2020. Effect of relative humidity on the carbonation rate of portlandite, calcium silicate hydrates, and ettringite. Cement and Concrete Research. 135, 106116. DOI: https://doi.org/10.1016/j.cemconres.2020.106116

[39] Silva, B.A., Ferreira Pinto, A.P., Gomes, A., et al., 2021. Effects of natural and accelerated carbonation on the properties of lime-based materials. Journal of CO2 Utilization. 49, 101552. DOI: https://doi.org/10.1016/j.jcou.2021.101552

[40] De Weerdt, K., Plusquellec, G., Revert, A.B., et al., 2019. Effect of carbonation on the pore solution of mortar. Cement and Concrete Research. 118, 38–56. DOI: https://doi.org/10.1016/j.cemconres.2019.02.004

[41] Wang, J., Su, H., Du, J., 2018. Influence of coupled effects between flexural tensile stress and carbonation time on the carbonation depth of concrete. Construction and Building Materials. 190, 439–451. DOI: https://doi.org/10.1016/j.conbuildmat.2018.09.117

[42] Bernal, S.A., Provis, J.L., Mejía de Gutiérrez, R., et al., 2015. Accelerated carbonation testing of alkali-activated slag/metakaolin blended concretes: Effect of exposure conditions. Materials and Structures. 48(3), 653–669. DOI: https://doi.org/10.1617/s11527-014-0289-4

[43] Seo, J., Kim, S., Park, S., et al., 2021. Carbonation of calcium sulfoaluminate cement blended with blast furnace slag. Cement and Concrete Composites. 118, 103918. DOI: https://doi.org/10.1016/j.cemconcomp.2020.103918

[44] Stewart, M.G., Teply, B., Králová, H., 2002. The effect of temporal and spatial variability of ambient carbon dioxide concentrations on carbonation of RC structures. In Proceedings of the 9th International Conference on Durability of Materials and Components, Brisbane, Australia, 17–20 March 2002.

[45] Sanjuán, M.A., del Olmo, C., 2001. Carbonation resistance of one industrial mortar used as a concrete coating. Building and Environment. 36(8), 949–953. DOI: https://doi.org/10.1016/S0360-1323(00)00045-7

[46] de Larrard, F., 1999. Concrete Mixtures Proportioning: A Scientific Approach. CRC Press: London, UK. DOI: https://doi.org/10.1201/9781482272055

[47] Standards Australia, 2009. AS3600-Concrete Structures. Standards Australia: Sydney, Australia.

[48] Lagerblad, B., 2005. Carbon Dioxide Uptake during Concrete Life Cycle: State of the Art. Swedish Cement and Concrete Research Institute: Stockholm, Sweden.

[49] CEB-FIP, 2010. Model Code for Concrete Structures. Fédération Internationale du Béton Lausanne, Switzerland.

[50] Dyer, T., 2014. Concrete Durability, 1st ed. CRC Press:

London, UK.
[51] Morinaga, S., 1988. Prediction of Service Lives of Reinforced Concrete Buildings Based on Rate of Corrosion of Reinforcing Steel (Special Report No. 23). Institute of Technology, Shimizu Corporation: Tokyo, Japan. (in Japanese)
[52] Idem, 1990. Prediction of service lives of reinforced concrete buildings based on the corrosion rate of reinforcing steel. In Proceedings of the 5th International Conference on Durability of Building Materials and Components, Brighton, UK. pp. 5–16.
[53] Bob, C., Afana, E., 1993. On-site assessment of concrete carbonation. In Proceedings of the International Conference Failure of Concrete Structures, Bratislava, Czechoslovakia. pp. 84–87.
[54] CEB-FIP, 1998. Strategies for Testing and Assessment of Concrete Structure: Guidance Report, Bulletin 243. CEB-FIP: Lausanne, Switzerland.
[55] CEB-FIP, 2006. Model Code for Service Life Design, Bulletin 34. Fédération Internationale du Béton/International Federation for Structural Concrete: Lausanne, Switzerland.
[56] CECS, 2007. CECS 220-Standard for Durability Assessment of Concrete Structures. China Architecture Industry Press: Beijing, China. (in Chinese)
[57] Jiang, L., Lin, B., Cai, Y., 2000. A model for predicting carbonation of high-volume fly ash concrete. Cement and Concrete Research. 30(5), 699–702. DOI: https://doi.org/10.1016/S0008-8846(00)00227-1
[58] Al-Ameeri, A.S., Rafiq, M.I., Tsioulou, O., et al., 2021. Impact of climate change on the carbonation in concrete due to carbon dioxide ingress: Experimental investigation and modeling. Journal of Building Engineering. 44, 102594. DOI: https://doi.org/10.1016/j.jobe.2021.102594
[59] Papadakis, V.G., Tsimas, S., 2002. Supplementary cementing materials in Concrete Part I: efficiency and design. Cement and Concrete Research. 32(10), 1525–1532. DOI: https://doi.org/10.1016/S0008-8846(02)00827-X
[60] Kwon, S.-J., Na, U.-J., 2011. Prediction of Durability for RC Columns with Crack and Joint under Carbonation Based on Probabilistic Approach. International Journal of Concrete Structures and Materials. 5(1), 11–18. Available from: https://koreascience.kr/article/JAKO201120956423767.pdf
[61] Silva, A., Neves, R., de Brito, J., 2014. Statistical modeling of carbonation in reinforced concrete. Cement and Concrete Composites. 50, 73–81. DOI: https://doi.org/10.1016/j.cemconcomp.2013.12.001
[62] Mizzi, B., Wang, Y., Borg, R.P., 2018. Effects of climate change on structures: analysis of carbonation-induced corrosion in Reinforced Concrete Structures in Malta. IOP Conference Series: Materials Science and Engineering. 442, 012023. DOI: https://doi.org/10.1088/1757-899X/442/1/012023
[63] Koichi, K., 1963. Durability of Iron Reinforced Concrete Structures. Kajima Construction Technology Research Institute Publishing Department: Tokyo, Japan. (in Japanese)
[64] Sisomphon, K., Franke, L., 2007. Carbonation Rates of Concretes Containing High Volume of Pozzolanic Materials. Cement and Concrete Research. 37(12), 1647–1653. DOI: https://doi.org/10.1016/j.cemconres.2007.08.014
[65] Aguayo, F., Torres, A., Kim, Y.-J., et al., 2020. Accelerated Carbonation Assessment of High-Volume Fly Ash Concrete. Journal of Materials Science and Chemical Engineering. 8, 23–38. DOI: https://doi.org/10.4236/msce.2020.83002
[66] Khunthongkeaw, J., Tangtermsirikul, S., Leelawat, T., 2006. A study on carbonation depth prediction for fly ash concrete. Construction and Building Materials. 20(9), 744–753. DOI: https://doi.org/10.1016/j.conbuildmat.2005.01.052
[67] Zhang, P., Li, Q.-F., 2013. Durability of high-performance concrete composites containing silica fume. Proceedings of the Institution of Mechanical Engineers Part L: Journal of Materials: Design and Applications. 227(4), 343–349. DOI: https://doi.org/10.1177/1464420712460617
[68] McGee, R., 1999. Modeling of Durability Performance of Tasmanian Bridges. In: Melchers, R.E., Stewart, M.G.S. (Eds.). ICASP8 Applications of Statistics and Probability in Civil Engineering. A.A. Balkema: Rotterdam, Netherlands. pp. 297–306.
[69] Teplý, B., Chromá, M., Rovnaník, P., 2010. Durability assessment of concrete structures: reinforcement de-passivation due to carbonation. Structure and Infrastructure Engineering. 6(3), 317–327.
[70] Rubinstein, R.Y., Kroese, D.P., 2016. Simulation and the Monte Carlo method. John Wiley & Sons: Hoboken, NJ, USA.
[71] Fishman, G., 2013. Monte Carlo: Concepts, Algorithms, and Applications. Springer Science & Business Media: New York, NY, USA. DOI: https://doi.org/10.1007/978-1-4757-2553-7
[72] Lemaire, M., 2013. Structural Reliability. John Wiley & Sons: London, UK.
[73] Hasofer, A.M., Lind, N.C., 1974. Exact and invariant second-moment code format. Journal of the Engineering Mechanics Division. 100(1), 111–121. DOI: https://doi.org/10.1061/JMCEA3.0001848
[74] Kabir, H., Wu, J., Dahal, S., et al., 2024. Automated estimation of cementitious sorptivity via computer vision. Nature Communications. 15, 9935. DOI: https://doi.org/10.1038/s41467-024-53993-w
[75] Song, Z., Zou, S., Zhou, W., et al., 2020. Clinically applicable histopathological diagnosis system for gastric cancer detection using deep learning. Nature Communications. 11, 4294. DOI: https://doi.org/10.1038/s41467-020-18147-8